Realization of a spin-1/2 Kondo necklace model with magnetic field-induced coupling switch

Hironori Yamaguchi [1,2] Yu Tominaga,[1] Takanori Kida,[3] Koji Araki,[4] Takashi Kawakami,[5] Yoshiki Iwasaki,[2,6]
Kenta Kimura [2,7] and Masayuki Hagiwara [3]

[1]*Department of Physics, Osaka Metropolitan University, Osaka 599-8531, Japan*
[2]*Innovative Quantum Material Center (IQMC), Osaka Metropolitan University, Osaka 599-8531, Japan*
[3]*Center for Advanced High Magnetic Field Science (AHMF), Graduate School of Science, Osaka University, Osaka 560-0043, Japan*
[4]*Department of Applied Physics, National Defense Academy, Kanagawa 239-8686, Japan*
[5]*Department of Chemistry, Osaka University, Osaka 560-0043, Japan*
[6]*Department of Physics, College of Humanities and Sciences, Nihon University, Tokyo 156-8550, Japan*
[7]*Department of Materials Science, Osaka Metropolitan University, Osaka 599-8531, Japan*

The theoretical Kondo necklace model, which simplifies the Kondo lattice model by focusing on spin degrees of freedom, provides a valuable framework for understanding spin-related quantum phenomena. However, it has not been applied to real materials until now. We present a realization of a spin-1/2 anisotropic Kondo necklace model using a complex of radical and Co spins. Electron spin resonance reveals anisotropic g values and an Ising-type exchange interaction with Co spin. The specific heat measurements demonstrate Schottky-type behavior, suggesting a Kondo singlet state with an energy gap in the excitation spectrum. Our findings suggest that a magnetic field can decouple Kondo interactions, unveiling a different mechanism for controlling Kondo coupling. This offers other opportunities for quantum technologies, particularly in the development of tunable qubits for quantum computing and spintronic devices, where precise control over spin interactions is essential.

The Kondo lattice model is a standard theoretical framework that describes low-temperature properties caused by the Kondo effect [1], resulting in heavy fermion behavior, quantum criticality, and unconventional superconductivity. The Kondo interaction induces a nonmagnetic singlet state by influencing the conduction electrons and localized spins. Ruderman-Kittel-Kasuya-Yosida (RKKY) interactions favor antiferromagnetic (AFM) long-range order. A quantum phase transition occurs between singlet and ordered states, with the Kondo-induced singlet being critical for modulating quantum dots [2–4], which presents a promising opportunity for quantum computing. The well-known Doniach diagram describes the competition between the Kondo effect and the RKKY interaction, illustrating how these interactions influence the magnetic and electronic properties of materials [5]. Magnetic fields and magnetic anisotropy not only shift the phase boundaries in the Doniach diagram but also lead to the emergence of new phases [6–9]. The Kondo necklace model, proposed by Doniach, is a simplified Kondo lattice model that focuses on the spin degree of freedom to realize a localized system [5]. Studies on spin-1/2 Kondo necklaces in one-dimensional (1D) systems show that finite Kondo interactions stabilize the quantum singlet state with a gap [10–15]. Numerical investigations suggest exotic quantum phases in anisotropic,

frustrated, and high-dimensional cases [16–18]. Understanding these phenomena provides insights into the effects of magnetic fields and anisotropy in the Doniach diagram, leading to the manipulation of the Kondo effect on conduction electrons and enabling innovative and precise control of band structures.

The diverse molecular structures of organic radicals can be used to specifically target localized spin systems. Using a triphenyl verdazyl radical, a verdazyl-based quantum organic material (V-QOM) was developed; V-QOM demonstrated multiple spin models not previously realized in conventional magnetic materials [19–21]. The application of V-QOM can be extended to complexes with 3d transition metals, leading to spin models consisting of intramolecular π-d coupling and intermolecular π-π stacking [22,23]. These complexes involve metal-radical coupling, magnetic anisotropy, and mixed spins, forming unique spin models. Notably, Co^{2+} in an octahedral crystal field leads to the formation of spin-1/2 models with anisotropic exchange interactions [24], serving as a platform for exploring unique quantum phases in anisotropic spin models.

In this Letter, we realize a spin-1/2 anisotropic Kondo necklace model in a $[Co(p$-Py-V$)(H_2O)_5] \cdot 2NO_3$ [p-Py-V = 3-(4-pyridinyl)-1,5-diphenylverdazyl] using a radical-based compound. Electron spin resonance analysis reveals anisotropic g values and an Ising-type exchange interaction associated with the Co spin. The specific heat measurements exhibit a clear Schottky-type behavior, indicating the formation of a Kondo singlet state with an excitation energy gap. Moreover, the observed magnetization curve
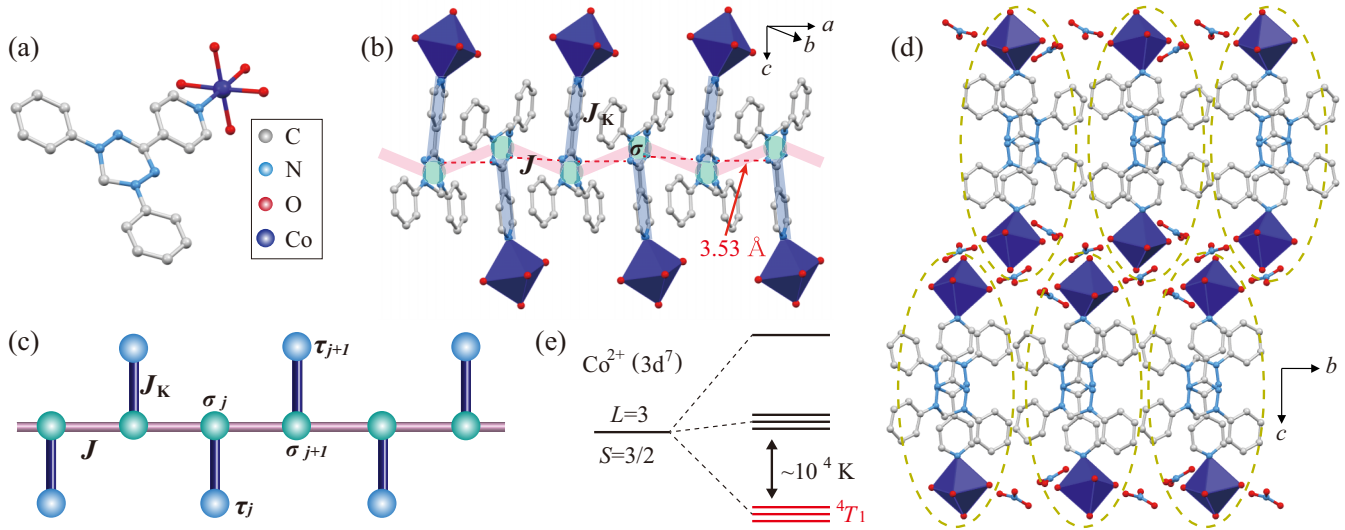
FIG. 1. (a) Molecular structure of Co(p-Py-V)(H_2O)$_5$, leading to an intramolecular exchange interaction J_K between the radical and Co spins. (b) Crystal structure forming the Kondo necklace model along the a axis. Hydrogen atoms are excluded to enhance clarity. The dashed lines indicate the N-N short contact associated with J. The green nodes represent the spin-1/2 of the radicals. The thick lines represent exchange interactions. (c) Spin-1/2 Kondo necklace model comprising J and J_K. σ and τ denote the spins on the radical and Co^{2+}, respectively. (d) Crystal structure observed in a direction parallel to the chain. The dashed line encloses molecules comprising each 1D structure. (e) Electronic configuration of high-spin Co^2 with $3d$ electrons leading to octahedral ligand field splitting, resulting in the formation of the lowest orbital triplet $^4T_1$.

demonstrates the decoupling of the Kondo interaction in the presence of a magnetic field, highlighting a different switching function of the Kondo coupling using the magnetic field.

The x-ray intensity data were collected using a Rigaku XtaLAB Synergy-S instrument. Magnetization measurements were conducted using a commercial superconducting quantum interference device (SQUID) magnetometer [magnetic property measurement system (MPMS), Quantum Design]. High-field magnetization in pulsed magnetic fields was measured using a nondestructive pulse magnet. A diamagnetic contribution calculated using Pascal's method was subtracted from the experimental data. The magnetization curve was corrected for the Van Vleck paramagnetism (0.008μ_B/Co^{2+}/T), which is determined to become constant above the saturation and close to the typical values reported for Co-based compounds [25,26]. Specific heat measurements were performed using a commercial calorimeter [physical property measurement system (PPMS), Quantum Design]. The electron spin resonance (ESR) measurement was performed using a vector network analyzer (ABmm), superconducting magnet (Oxford Instruments), and laboratory-built cylindrical cavity. All experiments were performed using powder samples. For the specific heat and ESR measurements, samples were fixed with grease to suppress the orientation in the external field direction. Molecular orbital (MO) calculations were performed using the unrestricted Becke three-parameter Lee-Yang-Parr functional (UB3LYP) method as broken-symmetry hybrid density functional theory calculations with a basis set of 6-31G(d,p). We employed a conventional evaluation scheme to estimate the intermolecular exchange interactions in the molecular pairs [27]. The quantum Monte Carlo (QMC) code is based on the directed loop algorithm in the stochastic series expansion representation [28]. The calculations was performed for $N = 512$ under the periodic boundary condition [29,30].

The molecular structure of Co(p-Py-V)(H_2O)$_5$ is shown in Fig. 1(a), with the cobalt (Co) atom surrounded by a pyridine in p-Py-V and five water (H_2O) ligand molecules, creating a six-coordinate environment. The verdazyl radical p-Py-V and Co^{2+} have spins of 1/2 and 3/2, respectively. In the p-Py-V molecule, the central ring comprises four nitrogen (N) atoms with a maximum spin density [19–21], leading to a localized spin system with intramolecular exchange interactions between the radical and Co spins. The crystallographic parameters at 100 K are as follows: monoclinic, space group P_{bca}, $a = 8.3851(4)$ Å, $b = 17.4265(9)$ Å, $c = 34.0707(15)$ Å, $V = 4978.5(4)$ Å^3, $Z = 8$ (see Supplemental Material [31]). Molecular orbital (MO) calculations were used to evaluate intermolecular exchange interactions between radicals, considering the spin-density distribution and MO overlap. Consequently, we found a predominant AFM interaction ($J/k_B = 9.3$ K), forming a spin-1/2 chain along the a axis, as shown in Fig. 1(b). The p-Py-V pair associated with J exhibits glide reflection symmetry and features an N-N short contact of 3.53 Å with a significant MO overlap. Each radical spin (σ) in the 1D chain is coupled with the Co spin (τ) via intramolecular interactions, yielding a Kondo necklace model composed of σ and τ, as shown in Figs. 1(b) and 1(c). The intramolecular interaction corresponds to the Kondo interaction, i.e., J_K, which was evaluated as $J_K/k_B = 10.5$ K. MO calculations tend to overestimate the intramolecular interactions between verdazyl radicals and transition metals; however, it is anticipated that the value of J_K will be in the order of several K (i.e., $J > J_K$) [22,23]. Moreover, the system exhibits no significant MO overlap and the nonmagnetic NO$_3$ serves as a spacer between the 1D structures, enhancing the 1D nature of the Kondo necklace model [Fig. 1(d)].
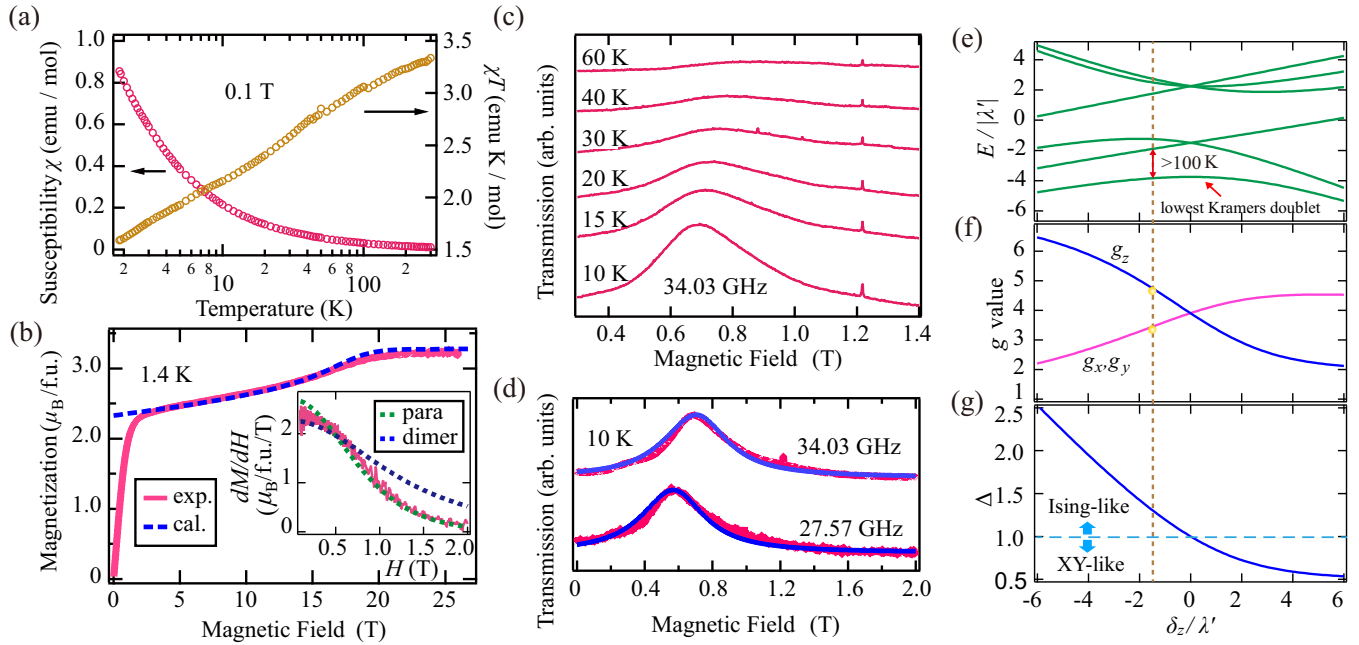
FIG. 2. (a) Temperature dependence of magnetic susceptibility ($\chi = M/H$) and χT of [Co(p-Py-V)(H$_2$O)$_5$] · 2NO$_3$ at 0.1 T. (b) Magnetization curve of [Co(p-Py-V)(H$_2$O)$_5$] · 2NO$_3$ at 1.4 K. For the spin-1/2 AFM chain, the dashed line represents the result calculated using the the QMC method with a radical purity of 95%. The calculated value has been shifted up by $2.66\mu_B$/f.u. considering the fully polarized Co spins. The inset shows the field derivative of the magnetization curve (dM/dH). The blue and green dashed lines represent the calculated result for the radical-Co dimer forming the Kondo singlet state and the Brillouin function for the paramagnetic Co spin at 1.4 K. (c) Temperature dependence of ESR absorption spectra of [Co(p-Py-V)(H$_2$O)$_5$] · 2NO$_3$ at 34.03 GHz. (d) Frequency dependence of ESR absorption spectra at 10 K. The solid lines represent the powder pattern simulation. (e) Splitting of the ground orbital triplet $^4T_1$ by the spin-orbit coupling λ' and the axial crystal field δ_z, as a function of δ_z/λ' with $k = 0.57$. (f) Corresponding g values for the ground Kramers doublets. The circles represent g values for the Co spin evaluated from the ESR analysis. (g) Expected anisotropy of the effective exchange interaction between the spins on the radical and Co^{2+} ion, i.e., J_K, in the low-temperature region. The horizontal line indicates an isotropic Heisenberg-type with a value of 1.0. The vertical line shows $\delta_z/\lambda' = -1.5$ for the present compound.

The effective spin of Co^{2+} was analyzed in a distorted octahedral environment in which high-spin Co^{2+} has total orbital and spin angular momenta of $L = 3$ and $S = 3/2$, respectively. Figure 1(e) shows a cubic crystalline electric field's ground state, which is an orbital triplet $^4T_1$. In this state, the fictitious orbital angular momentum $l = 1$ is used instead of the orbital angular momentum L. The introduction of spin-orbit coupling and crystal field distortion causes the $^4T_1$ ground state to split into six Kramers doublets [32,33], yielding a fictitious spin-1/2 (τ) with anisotropic g and exchange interactions at low temperatures. The magnetic anisotropy of Co^{2+} is strongly influenced by the magnitude of the crystal field distortion, leading to the creation of XY- or Ising-like systems [34,35] (see Supplemental Material [31]). The spin Hamiltonian of the proposed Kondo necklace model is given by

$$\mathcal{H} = J\sum_j \boldsymbol{\sigma}_j \cdot \boldsymbol{\sigma}_{j+1} + J_K \sum_j \left(\sigma_j^x \tau_j^x + \sigma_j^y \tau_j^y + \Delta \sigma_j^z \tau_j^z\right)$$

$$- g_\sigma \mu_B \sum_j H \cdot \boldsymbol{\sigma}_j - \mu_B \sum_j H \tilde{\mathbf{g}} \boldsymbol{\tau}_j, \qquad (1)$$

where Δ denotes axial anisotropy in the Kondo interaction, H denotes the external magnetic field, g_σ denotes the g of the radical spin, and $\tilde{\mathbf{g}}$ denotes the g tensor of the Co

spin. The diagonal components for the principal axes of the g tensor are g_x, g_y, and g_z and the other components are zero.

The relationship between magnetic susceptibility ($\chi = M/H$) and temperature at 0.1 T is shown in Fig. 2(a). The evolution of the AFM correlation is demonstrated by a decrease in χT with temperature despite a paramagneticlike increase in χ. The magnetization curve at 1.4 K [Fig. 2(b)] exhibits an increase up to a field of 1 T, above which the magnetization exhibits a nonlinear increase towards saturation at ~20 T. This highlights the nonlinear behavior typical of 1D quantum spin systems, which originates from the radical spins constituting the spin-1/2 Heisenberg AFM chain. Its ground state is known to be described as a Tomonaga-Luttinger liquid (TLL), which is a quantum critical state with fermionic spin-1/2 spinon excitations [36–38]. The increase in magnetization above 1 T actually corresponds to a magnetic moment attributed to a spin-1/2 with an isotropic g of 2.00, ~$1.0\mu_B$/f.u. We calculated the magnetization curve in terms of the spin-1/2 AFM chain through the QMC method. The calculated result reproduces the observed behavior for $H > 1$ T using $J/k_B = 12$ K, as shown in Fig. 2(b). Hence, the lower-field behavior originates from Co spins, indicating the full polarization of Co spins along the field direction for $H > 1$ T.

The magnetic behavior of Co^{2+} at low temperatures can be described as a fictitious spin-1/2 with anisotropic g,

considering the 3d orbital angular momentum degeneracy in an octahedral crystal field. During magnetization measurements, the samples were aligned with the external magnetic field because of their large magnetic anisotropy to detect magnetization along the easy axis [24]. The asymptotic value of 2.33μ_B/f.u. at ∼1 T indicates the saturation of spin-1/2 with $g_z = 4.66$. The ESR absorption spectrum in Fig. 2(c) shows a broad resonance, aligning with the anisotropic g of the Co spins. As the powder sample used in this measurement is restrained from orienting in the external field direction by mixing it with grease, the observed signals correspond to the powder pattern. At 1.22 T, distinct resonance signals indicate the presence of organic radical systems, confirming the isotropic properties of the verdazyl radical with $g_\sigma = 2.00$. The broad resonance signals in the lower-field region originate from Co spins and become prominent with decreasing temperature. Considering that the magnetic moment of the radical spin is strongly suppressed by the formation of the TLL, the resonance spectra in the low-temperature region are largely attributed to the Co spins. Figure 2(d) shows the ESR spectra at 10 K, with the Co spin remaining paramagnetic. Simulated ESR spectra assuming paramagnetic resonance with anisotropic g values accurately reproduced the observed line shape with $g_x = g_y = 3.35$ and $g_z = 4.66$.

We examined the evaluated magnetic anisotropy of Co^{2+} in the octahedral crystal field. The orbital degeneracy of the ground state orbital triplet $^4T_1$ is removed by the axial crystal fields, δ_z, leading to axial magnetic anisotropy. The Hamiltonian, derived from perturbative to spin-orbit coupling and crystal fields, is expressed as follows,

$$\mathcal{H} = \frac{3}{2}\lambda' \boldsymbol{l} \cdot \boldsymbol{S} - \delta_z\left(l_z^2 - \frac{2}{3}\right), \qquad (2)$$

where $\lambda' = k\lambda$, λ denotes the spin-orbit coupling constant, and k denotes the orbital reduction factor originating from the admixture between the 3d electron and p electrons in the ligands [32,33]. For hexa-coordinated high-spin Co^{2+}, typical values of λ and k are usually in the ranges of −180 to −130 cm^{-1} and 0.6–0.9, respectively [39,40]. By solving the secular equation, the energy states can be calculated as a function of δ_z/λ' while keeping other parameters constant [24] (see Supplemental Material [31]). The energy gap between the ground Kramers doublet and the first excited state, which is several hundred degrees K, enables the characterization of the magnetic properties at low temperatures using the doublet states [Fig. 2(e)]. Considering the energy shift of the Kramers doublet as the Zeeman splitting of an effective spin τ (fictitious spin-1/2), the g values were then evaluated for the principal axes. We explained the anisotropic g values evaluated from the ESR analysis using the parameters $\delta_z/\lambda' = -1.5$, and $k = 0.57$ [Fig. 2(f)]. The anisotropy of the exchange interaction between σ and τ, Δ, is presented in Fig. 2(g) as a function of δ_z/λ' [24], indicating that the complex exhibits Ising-type anisotropy with $\Delta = 1.3$.

Figures 3(a) and 3(b) show the relationship between temperature and specific heat. At zero field, a broad peak appears at ∼0.53 K, which is characteristic of Schottky-type behavior linked to the energy gap between excited states [41,42]. Applying a magnetic field shifts this peak to lower
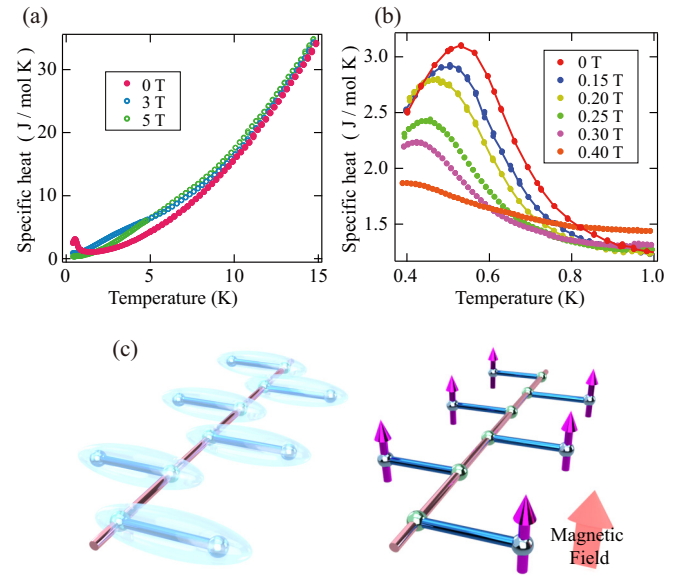

FIG. 3. (a), (b) Temperature dependence of the specific heat of [Co(p-Py-V)(H$_2$O)$_5$] · 2NO$_3$ at various magnetic fields. The lines are guides for the eye. (c) Valence bond picture of the Kondo singlet and field-induced states with decoupled Co spins in the Kondo necklace model. The oval shapes and arrows represent the valence bond singlet comprising σ and τ through J_K and fully polarized τ along the external field direction, respectively.

temperatures, indicating a reduced energy gap. Considering that a broad peak attributed to short-range AFM correlations is generally less affected by a magnetic field, this observed behavior indicates the formation of a Kondo singlet state stabilized by J_K [Fig. 3(c)]. At higher magnetic fields, the specific heat reflects the contributions of the fully polarized Co spin with the Zeeman gap and the AFM correlations of the TLL comprising radical spins. Assuming the AFM dimer coupled by anisotropic J_K [i.e., $J = 0$ in Eq. (1)], we calculated the eigenvalues by diagonalizing the spin Hamiltonian [43], revealing that the Schottky peak temperature of 0.53 K corresponds to $J_K/k_B = 1.4$ K (see Supplemental Material [31]). The discrepancy between the J_K values obtained from MO calculations and the experimental results can be attributed to the strong dependence of the choice of calculation method and basis set, resulting from the spin-orbit couplings of Co^{2+} [44]. Nonetheless, when compared to typical MO calculations involving 3d transition metals, the present values are reasonably close. From the field dependence of the eigenvalues, the critical field H_c where the energy gap closes for a magnetic field parallel to the easy axis, which is the case for the magnetization measurements, is derived as $\Delta J(g_\sigma + g_z) + J[4g_\sigma g_z + (g_\sigma - g_z)^2\Delta^2]^{1/2}/(4g_\sigma g_z\mu_B) \approx 0.9$ T. The disappearance of the energy gap is expected to cause a field-induced TLL state involving all spins that form the Kondo necklace model, similar to conventional 1D systems with a gap. However, the magnetic properties of the present system indicate a decoupling of radical and Co spins when the energy gap disappears, resulting in the phase transition from the radical-Co singlet state to the paramagnetic Co spin with the TLL of radical spins [Fig. 3(c)], that is completely different from conventional expected behavior. Although the experimental magnetization

curve in the vicinity of H_c exhibits a paramagneticlike behavior owing to the small energy scales of the gap and the critical field (see Supplemental Material [31]), the observed behavior of its field derivative dM/dH below H_c is indeed closer to the radical-Co dimer than the paramagnetic Co spin, as shown in the inset of Fig. 2(b). In the high-field region, the fully polarized Co spins have no degrees of freedom to modify the ground state, stabilizing the TLL state in the 1D AFM chain composed of radical spins without interference from the Co spins. We consider that the significant difference in the present g values between the spin sites connected by the Kondo interaction leads to the qualitative difference in the field-induced quantum behavior. The full polarization of the large magnetic moment causes a large energy gain in the magnetic field, leading to a decoupling of the Kondo interaction.

In summary, we synthesized a Co-based complex $[Co(p\text{-Py-V})(H_2O)_5] \cdot 2NO_3$ to develop a spin-1/2 anisotropic Kondo necklace model with radicals and Co spins. Experimental ESR and Co^{2+} spin-orbit coupling in a distorted octahedral environment were used to evaluate the anisotropic g and Ising-type exchange interactions. A clear Schottky-type behavior indicated the formation of a Kondo singlet state with an excitation energy gap. Further, applying a magnetic field decoupled the Kondo interaction, which is evident from the nonlinear magnetization curve, which is characteristic of a TLL. This mechanism can control quantum bits for quantum computing and conduction electron band structures, thereby creating opportunities for advanced sensors and innovative materials.

[1] J. Kondo, Resistance minimum in dilute magnetic alloys, Prog. Theor. Phys. **32**, 37 (1964).

[2] L. I. Glazman and M. E. Raikh, Resonant Kondo transparency of a barrier with quasilocal impurity states, Sov. JETP Lett. **47**, 452 (1988).

[3] D. Goldhaber-Gordon, H. Shtrikman, D. Mahalu, D. Abusch-Magder, U. Meirav, and M. A. Kastner, Kondo effect in a single-electron transistor, Nature (London) **391**, 156 (1998).

[4] S. M. Cronenwett, T. H. Oosterkamp, and L. P. Kouwenhoven, A tunable Kondo effect in quantum dots, Science **281**, 540 (1998).

[5] S. Doniach, The Kondo lattice and weak antiferromagnetism, Phys. B: Condens. Matter **91**, 231 (1977).

[6] T. A. Costi, Kondo effect in a magnetic field and the magnetoresistivity of Kondo alloys, Phys. Rev. Lett. **85**, 1504 (2000).

[7] M. Pustilnik and L. I. Glazman, Kondo effect induced by a magnetic field, Phys. Rev. B **64**, 045328 (2001).

[8] A. F. Otte, M. Ternes, K. von Bergmann, S. Loth, H. Brune, C. P. Lutz, C. F. Hirjibehedin, and A. J. Heinrich, The role of magnetic anisotropy in the Kondo effect, Nat. Phys. **4**, 847 (2008).

[9] M. Kanász-Nagy, Y. Ashida, T. Shi, C. P. Moca, T. N. Ikeda, S. Fölling, J. I. Cirac, G. Zaránd, and E. A. Demler, Exploring the anisotropic Kondo model in and out of equilibrium with alkaline-earth atom, Phys. Rev. B **97**, 155156 (2018).

[10] R. Jullien, J. N. Fields, and S. Doniach, Zero-temperature real-space renormalization-group method for a Kondo-lattice model Hamiltonian, Phys. Rev. B **16**, 4889 (1977).

[11] S. Moukouri, L. G. Caron, C. Bourbonnais, and L. Hubert, Real-space density-matrix renormalization-group study of the Kondo necklace, Phys. Rev. B **51**, 15920 (1995).

[12] H. Otsuka and T. Nishino, Gap-formation mechanism of the Kondo-necklace model, Phys. Rev. B **52**, 15066 (1995).

[13] G.-M. Zhang, Q. Gu, and L. Yu, Kondo spin liquid and magnetically long-range ordered states in the Kondo necklace model, Phys. Rev. B **62**, 69 (2000).

[14] F. H. L. Essler, T. Kuzmenko, and I. A. Zaliznyak, Luttinger liquid coupled to quantum spins: Flow equation approach to the Kondo necklace model, Phys. Rev. B **76**, 115108 (2007).

[15] J. J. Mendoza-Arenas, R. Franco, and J. Silva-Valencia, Gap formation and phase transition of the anisotropic Kondo necklace model: Density matrix renormalization group analysis, Phys. Rev. B **81**, 035103 (2010).

[16] T. Yamamoto, M. Asano, and C. Ishii, Magnetization process of one-dimensional Kondo necklace model with next-nearest-neighbor interaction, J. Phys. Soc. Jpn. **70**, 3678 (2001).

[17] T. Yamamoto, K. Ide, and C. Ishii, Phase diagram and critical properties of the frustrated Kondo necklace model in a magnetic field,, Phys. Rev. B **66**, 104408 (2002).

[18] W.-L. Tu, E.-G. Moon, K.-W. Lee, W. E. Pickett, and H.-Y. Lee, Field-induced Bose-Einstein condensation and supersolid in the two-dimensional Kondo necklace, Commun. Phys. **5**, 130 (2022).

[19] H. Yamaguchi, K. Iwase, T. Ono, T. Shimokawa, H. Nakano, Y. Shimura, N. Kase, S. Kittaka, T. Sakakibara, T. Kawakami, and Y. Hosokoshi, Unconventional magnetic and thermodynamic properties of $S = 1/2$ spin ladder with ferromagnetic legs, Phys. Rev. Lett. **110**, 157205 (2013).

[20] H. Yamaguchi, Y. Tamekuni, Y. Iwasaki, and Y. Hosokoshi, Candidate for a fully frustrated square lattice in a verdazyl-based salt, Phys. Rev. B **97**, 201109(R) (2018).

[21] H. Yamaguchi, Y. Iwasaki, Y. Kono, T. Okubo, S. Miyamoto, Y. Hosokoshi, A. Matsuo, T. Sakakibara, T. Kida, and M. Hagiwara, Quantum critical phenomena in a spin-1/2 frustrated square lattice with spatial anisotropy, Phys. Rev. B **103**, L220407 (2021).

[22] H. Yamaguchi, S. C. Furuya, S. Morota, S. Shimono, T. Kawakami, Y. Kusanose, Y. Shimura, K. Nakano, and Y. Hosokoshi, Observation of thermodynamics originating from a mixed-spin ferromagnetic chain, Phys. Rev. B **106**, L100404 (2022).

[23] H. Tsukiyama, S. Morota, S. Shimono, Y. Iwasaki, M. Hagiwara, Y. Hosokoshi, and H. Yamaguchi, Crystal structures and magnetic properties of verdazyl-based complexes with transition metals, Phys. Rev. Mater. **6**, 094417 (2022).

[24] H. Yamaguchi, Y. Tominaga, A. Matsuo, S. Morota, Y. Hosokoshi, M. Hagiwara, and K. Kindo, Ladder-based two-dimensional spin model in a radical-Co complex, Phys. Rev. B **107**, 174422 (2023).

[25] Y. Kojima, M. Watanabe, N. Kurita, H. Tanaka, A. Matsuo, K. Kindo, and M. Avdeev, Quantum magnetic properties of the spin-1/2 triangular-lattice antiferromagnet $Ba_2La_2CoTe_2O_{12}$, Phys. Rev. B **98**, 174406 (2018).

[26] X. C. Liu, Z. W. Ouyang, T. T. Xiao, J. J. Cao, Z. X. Wang, Z. C. Xia, Z. Z. He, and W. Tong, Magnetism and ESR of the $S_{eff} = 1/2$ antiferromagnet $BaCo_2(SeO_3)_3 \cdot 3H_2O$ with dimer-chain structure, Phys. Rev. B **105**, 134417 (2022).

[27] M. Shoji *et al.*, A general algorithm for calculation of Heisenberg exchange integrals J in multispin systems, Chem. Phys. Lett. **432**, 343 (2006).

[28] A. W. Sandvik, Stochastic series expansion method with operator-loop update, Phys. Rev. B **59**, R14157 (1999).

[29] A. F. Albuquerque *et al.*, The ALPS project release 1.3: Open-source software for strongly correlated systems, J. Magn. Magn. Mater. **310**, 1187-1193 (2007).

[30] B. Bauer *et al.*, The ALPS project release 2.0: open source software for strongly correlated systems, J. Stat. Mech. **2011**, P05001 (2011).

[31] See Supplemental Material at http://link.aps.org/supplemental/10.1103/PhysRevResearch.7.L012023 for the details of the crystal structure, ESR analysis, magnetic anisotropy evaluation, and magnetic properties of the radical-Co dimer.

[32] A. Abragam and M. H. L. Pryce, The theory of paramagnetic resonance in hydrate cobalt salts, Proc. R. Soc. London, Ser. A **206**, 173 (1951).

[33] M. E. Lines, Magnetic properties of $CoCl_2$ and $NiCl_2$, Phys. Rev. **131**, 546 (1963).

[34] S. K. Satija, G. Shirane, H. Yoshizawa, and K. Hirakawa, Neutron scattering study of spin dynamics in $CsCoCl_3$, Phys. Rev. Lett. **44**, 1548 (1980).

[35] S. Kimura, H. Yashiro, K. Okunishi, M. Hagiwara, Z. He, K. Kindo, T. Taniyama, and M. Itoh, Field-induced order-disorder transition in antiferromagnetic $BaCo_2V_2O_8$ driven by a softening of spinon excitation, Phys. Rev. Lett. **99**, 087602 (2007).

[36] S. Tomonaga, Remarks on Bloch's method of sound waves applied to many-fermion problems, Prog. Theor. Phys. **5**, 544 (1950).

[37] J. M. Luttinger, An exactly soluble model of a many–fermion system, J Math. Phys. **4**, 1154 (1963).

[38] T. Giamarchi, *Quantum Physics in One Dimension*, International Series of Monographs on Physics (Oxford Science/Clarendon, Oxford, UK, 2004).

[39] D. V. Korchagin, A. V. Palii, E. A. Yureva, A. V. Akimov, E. Y. Misochko, G. V. Shilov, A. D. Talantsev, R. B. Morgunov, A. A. Shakin, S. M. Aldoshin, and B. S. Tsukerblat, Evidence of field induced slow magnetic relaxation in *cis*-$[Co(hfac)_2(H_2O)_2]$ exhibiting tri-axial anisotropy with a negative axial component, Dalton Trans. **46**, 7540 (2017).

[40] F. Lloret, M. Julve, J. Cano, R.-R. Carcía, and E. Pardo, Magnetic properties of six-coordinated high-spin cobalt(II) complexes: Theoretical background and its application, Inorg. Chim. Acta **361**, 3432 (2008).

[41] Y. Yoshida, N. Tateiwa, M. Mito, T. Kawae, K. Takeda, Y. Hosokoshi, and K. Inoue, Specific heat study of an $S = 1/2$ alternating Heisenberg chain system: F_5PNN in a magnetic field, Phys. Rev. Lett. **94**, 037203 (2005).

[42] Ch. Rüegg, K. Kiefer, B. Thielemann, D. F. McMorrow, V. Zapf, B. Normand, M. B. Zvonarev, P. Bouillot, C. Kollath, T. Giamarchi, S. Capponi, D. Poilblanc, D. Biner, and K. W. Krämer, Thermodynamics of the spin Luttinger liquid in a model ladder material, Phys. Rev. Lett. **101**, 247202 (2008).

[43] Y. Nakagawa, T. Kashiwagi, H. Yamaguchi, S. Kimura, Z. Honda, K. Yamada, K. Kindo, and M. Hagiwara, High field ESR and magnetization in $Na_2Co_2(C_2O_4)_3(H_2O)_2$, J. Phys. Soc. Jpn. **75**, 124708 (2006).

[44] L. Freitag, S. Knecht, C. Angeli, and M. Reiher, Multireference perturbation theory with Cholesky decomposition for the density matrix renormalization group, J. Chem. Theory Comput. **13**, 451 (2017).